International Journal of Latest Engineering and Management Research (IJLEMR)
ISSN: 2455-4847
www.ijlemr.com || Volume 08 – Issue 05 || May 2023 || PP. 56-69

Numerical study of reasonable cycle step length for longwall top-coal drawing in extra-thick coal seams based on the particle-block element coupling approach

Yaochuang Wang
[1](Zhongyun International Engineering Co., Ltd, Zhengzhou, 450000, China)
[2] (School of Energy Science and Engineering, Henan Polytechnic University, Jiaozuo, 454003, China)

Abstract: The cycle step length (CSL) is a significant parameter for longwall top-coal drawing technology that remarkably affects the top-coal recovery rate and the rock-mixing rate, especially for extra-thick coal seams. In this study, a particle-block element coupling approach is performed to investigate a reasonable CSL for extra-thick coal seams. By comparing this approach to the Bergmark-Roos analytical result, the proposed numerical model is verified, showing good performance in modeling top-coal caving. A 2-D numerical model of hydraulic support considering the mechanical behavior of the legs is established, which can be used for modeling the interaction between the hydraulic support and the top coals during the top-coal drawing process. The top-coal recovery rate, the top-coal drawing body shape, and the evolution characteristics of the coal-rock interface under different CSL conditions are compared. In addition, the mechanism of the lost top coal affected by the CSL is revealed. The results show that the CSL of top-coal drawing has a significant effect on the morphology of the coal-rock interface and the mutual invasion of coal and rock, which is the primary reason for coal loss and further affects the top-coal recovery rate and the rock-mixing rate. It is suggested that the CSL should be 0.8 m when the top-coal thickness is 12 m.

Keywords: Coal-rock interface, cycle step length, particle-block element, top-coal drawing process, top-coal recovery rate

1. Introduction

Coal resources will still play a pivotal role in the proportion of energy consumption in the future. In China, thick coal seams (thickness ≥3.5 m) account for approximately 45% of the total coal reserves. There are three mining techniques used for thick coal seams: longwall fully mechanized mining with a large cutting height, longwall fully mechanized top-coal caving (LTCC), and slicing mining. As early as the early 20th century, LTCC was first applied in the Blanche coal mine in France, but it was only used for special mining in steep coal seams, corner coal, coal pillars, and other complex geological environments. Thereafter, the former Soviet Union, Romania, Spain, the former Yugoslavia, Hungary, and other countries gradually began to formally study the applicability of LTCC in thick coal seams. In China, LTCC began in the 1980s but developed rapidly. At present, LTCC has gradually become the most popular method for mining thick or extra-thick coal seams[1][2][3], and China is in the leading position in the world in studying automated LTCC technology[4][5][6]. In traditional top-coal mining technology, the drawing process is observed by workers through a gap between hydraulic supports. “Rocks appear at the coal drawing opening” is commonly regarded as the criterion for terminating the coal drawing. However, because of the hysteresis of the closing action response under manual operation, the top coal will still flow out with many rocks before the openings are closed, resulting in a high rock-mixing rate. With the introduction of automation and artificial intelligence technology into the mining industry, more than 100 longwall working faces have been equipped with automated and intelligent coal cutting technologies (e.g., automatic alignment technology of the working face and distinguishing technology of coal and rock)[7][8][9][10]. However, the high rock-mixing rate and low top-coal recovery rate (most are lower than 65% in extra-thick coal seams) are still outstanding problems for LTCC. It is widely thought that the CSL is significantly related to the above two rates[11], but the influence mechanism of the CSL remains unclear.

The theoretical study of LTCC in China lags behind its engineering application. In the early stage, the top-coal caving and flow laws are attracted. Wu et al. introduced the ellipsoid theory of metal ore caving into the study of top-coal drawing to explore the shape of the top-coal drawing body and put forward the ellipsoid theory for coal drawing [12][13][14]. Since 2000, low-level caving hydraulic support has been widely used in China. Through simulation tests, numerical analysis, and field observations, Wang et al. proposed the theory of granular medium flow for top-coal drawing, considering the influences of the CSL, shield beam, and tail beam on hydraulic support. Then, the boundary-body-ratio (BBR) research system was established to study the four factors of the coal-rock interface, top-coal drawing body, top-coal recovery rate, and rock-mixing

rate[15][16][17][18]. Numerical simulation has also developed rapidly into an effective method for studying LTCC. Khanal [19][20] established a numerical LTCC model with COSFLOW software and analyzed the support collapse, top coal failure mechanism, roof caving mechanism, support stress, and vertical stress on the caving effect and finally discussed the feasibility of using LTCC technology in the Adriyala coal mine. In addition, the finite difference method was used to analyze the mechanism of top-coal caving in the Omerler coal mine [4][21]. Using PFC2D, Xie and Zhao [3] proved that the top-coal arch structure can be caused only by gravity conditions and is easily damaged by vibration. Wang et al. [22][23] performed PFC3D to study the influence of hydraulic support on the shape of the top-coal drawing body and believed that the top-coal drawing body was a variant ellipsoid cut by the shield beam of hydraulic support. Liu et al. [24] used CDEM software to study the coal drawing methods and evolution characteristics of the coal-rock interface at the different stages of initial coal caving, intermediate coal caving, and end coal caving under the condition of multiple top-coal drawing openings. Zhang et al. [25] studied the law of fully mechanized top-coal caving mining in extra-thick coal seams based on the continuous medium discontinuous element method.

Because of the complex environment behind hydraulic supports, it is difficult to observe the top-coal caving process above the hydraulic support. A numerical simulation is thus a fast and effective way to simulate the top-coal caving process. The particle element method is the major simulation method used for studying top-coal drawing, but modeling the interaction between the hydraulic support and the top coal during the drawing process presents a challenge. In this study, the particle-block element coupling approach is used to simulate the longwall top-coal drawing process. The block mesh model and the constitutive law of hydraulic support are proposed, and the interaction principle between particles and block elements is introduced. The process of top-coal drawing with a single coal drawing opening is modeled and verified with the Bergmark-Roos analytical model. Then, the correlation between the top-coal recovery rate and the shape of the coal-rock interface is analyzed, and based on this result, a reasonable CSL for extra-thick coal seams is determined.

2. Governing equations

2.1 The interaction principle between particle and block element

In a numerical simulation method of top-coal mining, the flow of particles from aggregates broken into loose and falling particles can well simulate the top-coal drawing process and the coal-rock interface state. In addition, a hydraulic support numerical model is added to the simulation process. The block element can accurately simulate and analyze the stress state of the coal rock and hydraulic support so that the simulation result of the top-coal drawing process is closer to the actual situation of the project. The calculation principle of particle and block coupling used in this paper is as follows[26][27][28][29].

The internal mechanical calculation of the block element adopts the explicit solution method to calculate the finite element, including the calculation of the element node force and the calculation of the element node motion

The calculation formula of the resultant force on the element node is as follows:

$$F = F_e + F_d + F_c \quad (1)$$

Where F is the resultant force of the element node, F_e is the external force of the element node, F_D is the deformation force of the element node, and F_C is the damping force of the element node.

The calculation formula of node movement is as follows:

$$a = F/m \quad (2\text{-}1)$$
$$v = \sum_{t=0}^{Tnow} a \cdot \Delta t \quad (2\text{-}2)$$
$$\Delta u = v \cdot \Delta t \quad (2\text{-}3)$$
$$u = \sum_{t=0}^{Tnow} \Delta u \quad (2\text{-}4)$$

Where a is the acceleration of the node of the calculation element; v is the velocity of the node of the calculation element; Δu is the displacement increment of the node of the calculation element; $u$is the full amount of the node displacement of the calculation element; m is the mass of the node of the calculation element; and Δt is the node of the calculation element time step.

Using the incremental calculation method to calculate the stress of the element and the node deformation of the element gives the following:

$$\{\Delta\xi\}_i = [B]_i \cdot \{\Delta u\}_e \quad (3\text{-}1)$$
$$\{\Delta\sigma\}_i = [D]_i \cdot \{\Delta\xi\}_i \quad (3\text{-}2)$$
$$\{\Delta\sigma\}_i = \{\sigma^0\}_i + \{\Delta\sigma\}_i \quad (3\text{-}3)$$
$$\{F_n\}_e = \sum_{i=1}^{N} [B]_i^T \cdot \{\sigma^n\}_i \cdot \omega_i \cdot J_i \quad (3\text{-}4)$$

Where$[B]_i$, $\{\Delta\xi\}_i$, $\{\Delta\sigma\}_i$, ω_i, and J_i are the strain calculation matrix of Gaussian point i, the vector of incremental strain, the vector of incremental stress, the integral coefficient and the Jacobian determinant; $\{\Delta\sigma^n\}_i$and $\{\sigma^0\}_i$ are the total stress at the current time and the previous time of Gaussian point i for the

calculation element;$[D]$,$\{\Delta u\}_e$, and $\{F_d\}_e$ are the elastic matrix of the calculation element, the displacement vector of the incremental node of the calculation element and the vector of the node force of the calculation element; *N* is the number of Gaussian points.

The linked bar model can be used to simulate the continuous medium properties between the particles. A connecting rod model is established between the two particle elements, as shown in Fig 1. It is used to simulate the process from the initial intact state to crushing of the top-coal drawing. The link bar model is regarded as a rectangle, through which the contact force or cohesive force between the two particle elements can be calculated. The long side of the rectangle is the sum of the radii of the two particles, while the short side is equal to the diameter of the smaller particles. Based on the connecting rod model, the relationship between the two particle elements is the surface contact, and the equivalent contact area A_C is the projected area of the smaller particles.

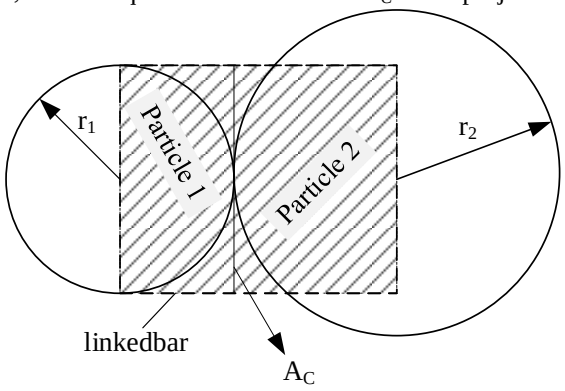

Figure1Thelinked bar model

The formula for calculating the contact force between the discrete elements of the particles is as follows:

$$F_n(t+\Delta t) = F_n(t) - K_n \Delta u_n \quad (4\text{-}1)$$

$$F_s(t+\Delta t) = F_s(t) - K_s \Delta u_s \quad (4\text{-}2)$$

WhereΔu_n and Δu_s are the incremental difference of the normal displacement and the incremental difference of the tangential displacement between two discrete elements of particles in contact with each other.
The formula for calculating the contact torque between discrete elements of particles is as follows:

$$M_n(t+\Delta t) = M_n(t) - K_s J \Delta\theta / A_c \quad (5\text{-}1)$$

$$M_s(t+\Delta t) = M_s(t) - K_n I \Delta\theta_s / A_c \quad (5\text{-}2)$$

Where M_n and M_s are the torque and bending moment between the discrete elements of the particles, *I* and *J* are the moment of inertia and the moment of inertia between the contact surfaces of the discrete elements of the particles, and $\Delta\theta$ and $\Delta\theta_s$ are the incremental differences between the torsion and bending angles between the discrete elements of the particles.

$$J = \pi(R_1 + R_2)^4/32 \quad (6\text{-}1)$$

$$I = J/2 \quad (6\text{-}2)$$

$$A_c = min(2R_1,\ 2R_2) \quad (6\text{-}3)$$

Where R_1 and R_2 are the radius values of the two particles contacting each other between the discrete elements of the particles, and A_c is the contact area between the discrete elements of the particles. The contact stiffness between the discrete elements of the particles can be derived from the elastic modulus and shear modulus of the particles in contact with each other:

$$K_n = \bar{E} A_c/(R_1 + R_2) \quad (7\text{-}1)$$

$$K_s = \bar{G} A_c/(R_1 + R_2) \quad (7\text{-}2)$$

Where K_n andK_s are the normal and tangential stiffness $\bar{E}$ between the discrete elements of the particles in contact with each other, and $\bar{G}$ is the average elastic modulus and the shear modulus of the two discrete elements of the particles in contact with each other.

According to the Mohr-Coulomb criterion and the maximum tensile stress criterion, the contact force calculation formula is as follows:

$$If\ -F_n - TA_c \geq 0,\ then\ F_n = F_s = 0,\ T = C = 0$$

$$If\ F_s - F_n \tan\varphi - CA_c \geq 0,\ then\ F_n = F_s \tan\varphi = 0,\ T = C = 0 \quad (8)$$

The contact judgment condition between the two particle elements is formula (9). If any one of the inequalities in the formula is satisfied, the contact between the particles will no longer transmit torque.

$$\left(\frac{-F_n}{A_c} + \frac{M_s}{I} R_{ave}\right) - T \geq 0;\ or$$

$$\left(\frac{|F_s|}{A_c}+\frac{M_s}{I}R_{ave}\right)-[F_n\ tan\,\varphi+C]\geq 0 \quad (9)$$

Where $R_{ave}=(R_1+R_2)/2$, T, C, and φ are the tensile strength, cohesion and internal friction angle, respectively, and I is the moment of inertia.

The calculation of the torque on the particle discrete element is as follows:

$$\Delta d=(\omega_1\omega_1-\omega_2\omega_2)\Delta t+(v_1-v_2)\Delta t \quad (10)$$

Where ω_1 and ω_2 are the vectors of the rotational angular velocity of particle discrete elements 1 and 2; r_1 and r_2 are the vectors of the relative positions of particle discrete elements 1 and 2 to the contact point (from the particle centroid to the contact point); and v_1 and v_2 are the translational velocity vectors of the centroid of particle discrete elements 1 and 2.

$$M_1=r_1F^{(G)};\ M_2=-r_2F^{(G)} \quad (11)$$

Where M_1 and M_2 are the torque on particle discrete elements 1 and 2, respectively, and $F^{(G)}$ is the contact force of the particle discrete element in the global coordinate system.

The core of the coupling calculation of the block element and the particle discrete element is the logical judgment of the mutual contact between the block element and the particle discrete element. In the two-dimensional numerical calculation, the method for judging the contact between the block element and the particle discrete element is the body center of the particle element. To judge the relative position of contact with the edge of the block element, the contact between the body center of the particle element and the edge of the block element must also satisfy that the distance from the body center of the particle discrete element to the boundary edge of the block element is less than or equal to the radius of the particle discrete element. That is $d\leq R$, and the projection point of the body center of the discrete element of the particle on the boundary edge of the block element is inside the edge of the block element, that is, $d_{ik}\leq d_{ij}$, $d_{jk}\leq d_{ij}$ can be established. Once the particle discrete element and the edge of a boundary block element have established a contact relationship, the normal spring and tangential spring that contact each other between the block element and the particle discrete element are automatically created, and the block element contacts the particle discrete element. The interpolation coefficient of point *k* will be automatically calculated by the following formula:

$$d=|V_{ki}\cdot n| \quad (12\text{-}1)$$

$$\omega_i=d_{jk}/d_{ij} \quad (12\text{-}2)$$

$$\omega_j=d_{ik}/d_{ij} \quad (12\text{-}3)$$

Where V_{ki} is the relative position vector of the particle from the element center *k* and the block element edge *i*, *i* and *j* are the two endpoints of the block edge, d_{jk} is the distance between point *j* and point *k*, d_{ij} is the difference between point *i* and point *j*, dik is the distance between point *i* and point *k*, and *n* is the normal vector outside at the edge of the block.

According to the alternating cycle calculation process of the theoretical formula (1~12), the explicit solution process for the finite element, discrete element, particle, and block coupling can be realized.

2.2 The constitutive law of hydraulic support

In previous simulation methods for top-coal drawing, most scholars used PFC to simulate the top-coal drawing process. To more realistically simulate the top-coal drawing process at the top-coal drawing working face, the constitutive model of the top-coal hydraulic support is put into the CDEM simulation.According to the coupling principle of block and particle introduced in Section 2.1, the interaction between the coal gangue particles and the hydraulic support for the top-coal drawing and the change process of the working resistance of the hydraulic support during the top-coal drawing process are simulated to more truly simulate the on-site coal caving process. The test points are arranged between the inner and outer columns of the hydraulic support, as shown in Fig.2(a). The red point is the measuring point of the working resistance of the hydraulic support for top-coal drawing. The hydraulic support model adopts the constitutive model, which can represent the relationship between the column shrinkage and the working resistance. The calculation formula is as follows:

$$P_1=P_0+K\Delta S \quad (13)$$

Where *P* is the working resistance of the support; P_0 is the setting force of the support; *K* is the hydraulic stiffness; ΔS is the shrinkage of the column.

The numerical constitutive curve of the hydraulic support is shown in Fig. 2(b) [30]. Fig.(b) shows that the constitutive structure of the stent in the simulation has two stages. In the first stage, the support resistance from the initial support force P_0 to the working resistance P_1 with stiffness *K* linearly increases as the column shrinks down. The safety valve opens in the second stage, and the working resistance of the support will not change as the column continues to shrink. As the working face advances, the hydraulic support is recycled from the above process.

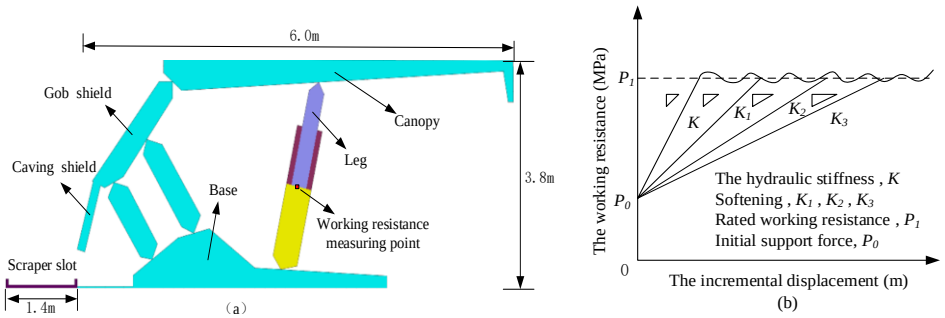

Fig. 2 (a) Numerical model and arrangement of measuring pointsand (b) numerical constitutive curve of support

3. Validation for the proposed particle approach

3.1 The Bergmark-Roos model

Here, we adopt the Bergmark-Roos analytical model to benchmark the proposed particle approach. The top coal is disturbed by mining and is broken into blocks under the combined action of the overlying rock layer and the hydraulic support. It is discharged through the drawing opening at the rear of the hydraulic support. However, the coal mining process on the cross-section parallel to the working face is not affected by the structure of the hydraulic support. Therefore, the top-coal drawing theory of a single drawing opening parallel to the cross-section of the working face can be interpreted by the Bergmark-Roos theory[31][32][33].

The Bergmark-Roos model mainly assumes that the broken top coal moves from a static straight line to the top-coal drawing opening. During the top-coal drawing process, the broken top coal is only affected by gravity and friction. During the top-coal drawing process, the acceleration of a single crushing top coal block is constant. The architecture of the Bergmark-Roos model is shown in Fig.3 (a).

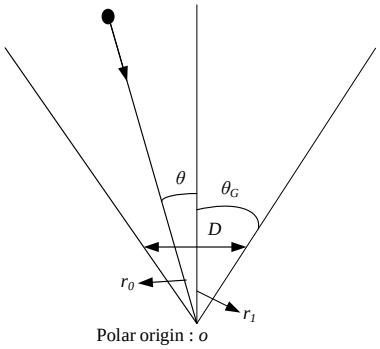

(a) Architecture of the Bergmark-Roos model

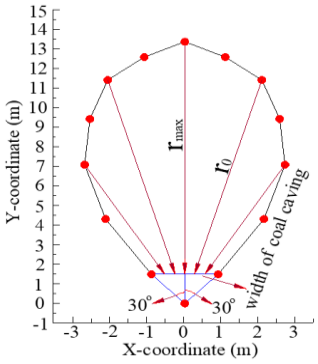

(b) theory model

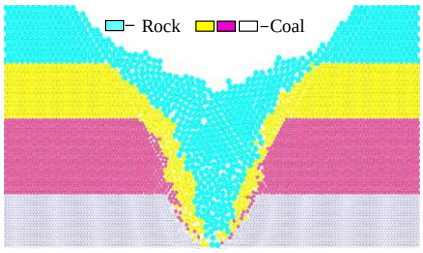

(c) The coal-rock interface after coal drawing

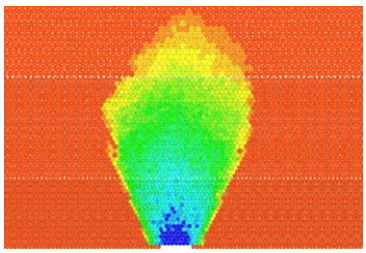

(d) Top coal caving body diagram

Figure 3 Comparison between the theoretical model and the numerical results of the top-coal drawing body

The boundary equation of the top-coal drawn in the polar coordinate system is as follows:

$$r_0 = (r_{max} - r_1)\frac{\cos\theta - \cos\theta_G}{1 - \cos\theta_G} + r_2 \quad (14)$$

According to Fig. 3(a), the distance from the origin of the coordinates to any point on the opening on the drawing is as follows:

$$r_2 = \frac{r_1}{\cos\theta} = \frac{D}{2\tan\theta_G \cos\theta} \quad (15)$$

Where

$$r_1 = \frac{D}{2\tan\theta_G} \quad (16)$$

Putting equations (15) and (16) into (14), we obtain:

$$r_0 = \left(r_{max} - \frac{D}{2\tan\theta_G}\right)\frac{\cos\theta - \cos\theta_G}{1-\cos\theta_G} + \frac{D}{2\tan\theta_G\cos\theta} \quad (17)$$

Where r_1 is the distance from the center of the drawing opening to the origin of the polar coordinates; r_2 is the distance from any point on the drawing opening to the origin of the polar coordinates; θ is the angular coordinate of the particle; θ_G is the maximum allowable displacement boundary angle. The force is equal to the angle of the particle weight; when $\theta = 0$, r_{max} is the maximum distance from the origin of polar coordinates to the boundary of the drawing body; and D is the size of the opening in the figure.

3.2 Comparison

According to the real dimension of the drawing opening, a 1.75 m wide opening is set at the bottom of the model to simulate the coal drawing opening. The top coals are fully broken before being drawn out. Therefore, the top coal strength parameter is set to 0 in this simulation. The termination condition for the end of coal drawing is "rocks appear, close the opening". As shown in Fig.3 (c), the coal-rock interface is funnel-shaped after top-coal drawing at a single coal drawing opening. To study the shape, trajectory and initial position of the loose body discharged through the coal drawing port, the numerical simulation adopts the method of reverse marking the position of the drawing body in the original mold at a specific time after recovering the loose body. In Fig. 3 (d), particles with the same color in the model are obtained by the reverse marking of a loose body released within a period, and the shape of top-coal released resembles an approximate ellipsoid state. Some particle coordinates are extracted from the ellipsoid boundary of Fig. 3 (d) to describe the development of the top-coal drawing body shape during top-coal drawing.

According to the ellipsoid theoretical simulation equation of formulas (16) and (17), the single coal drawing port model shows that the thickness of the top coal is r_1=12 m, and the size of the coal drawing opening is d = 1.75 m. From the numerical simulation of a single coal drawing opening, θ_G=30° can be obtained, and equation (17) is simplified to equation (18):

$$r_0 = \frac{12(2\cos\theta - \sqrt{3})}{2-\sqrt{3}} + \frac{7\sqrt{3}}{8\cos\theta} \quad (18)$$

According to formula (18), the theoretical model of the shape of the top-coal drawing body parallel to the cross-section of the working face is shown in Fig. 3(a). As shown in Fig. 3 (c), the top coal in the ellipsoid range can be finally discharged through the coal drawing port. Some of the top-coal particles outside the ellipsoid boundary are loose and not drawn out.

4 Numerical Model

4.1 Determination of numerical model parameters

The coal seam thickness of the no. 8222 fully mechanized top-coal caving panel in the Tashan coal mine is 8.17-29.21 m, with an average of 15.76 m; it has a mining height of 3.8 m and a utilization thickness of 7.81-22.11 m, with an average of 15.6 m, and a direct roof thickness of 1.51-14.52 m, with an average of 8.22 m. According to a geological report, the fractures of the coal seams are well-developed, and it exhibits a fragmentary uneven ladder-shaped fracture and has developed endogenous fractures. The coal is loose in structure, brittle and fragile, the joint spacing is 15 ~ 25 cm, and therefore the top coal is easily drawn out. To ensure the cutting depth and effective moving distance, the ZF17000/27.5/42D top-coal drawing hydraulic support was adopted. The stroke of the pushing jack of the support is 1120 mm. The height of the support is 2.75-4.2 m. The yield resistance of the hydraulic support is 17000 KN and its off-loading strength of the safety valve is 41.8 MPa. The working parameters of the support is shown in Table 1 below. To create the hydraulic support model, the simplified initial support diagram is first established with a height of 3.8 m in AutoCAD software, as shown in Fig. 2(a). According to the actual size of the hydraulic support in Fig. 2(a) and the specific position of the rear scraper conveyor, the coupling mesh model of the hydraulic support is created by ANSYS and CDEM software, as shown in Fig. 4. Under the condition of a 12.0 m top-coal thickness, a numerical model of a 6 m rock gangue layer in the upper part of the top coal is established to simulate crushing of the immediate roof. Along the strike of the working face, the length of the numerical model is 118 m. To eliminate the influence of the rigid boundary on the top-coal drawing body, a boundary width of 25 m is set on the left and right sides. The particle mechanics parameters, particle size, and layer height parameters used in the numerical simulation are shown in Table 2 and Fig. 4.

Table 1 The parameter values of ZF17000/27.5/42D type top-coal drawing hydraulic support

model	Working parameters	
ZF17000/27.5/42D Type caving support	Support structure height	2750~4200 mm
	Bracket width	1660~1860 mm
	Center distance of bracket	1750 mm
	CSL	1000 mm
	Initial support force	12778kN (31.4 MPa)
	Rated working resistance	17000kN (41.8 MPa)
	Support strength	1.45 MPa
	Pump station pressure	31.4 MPa

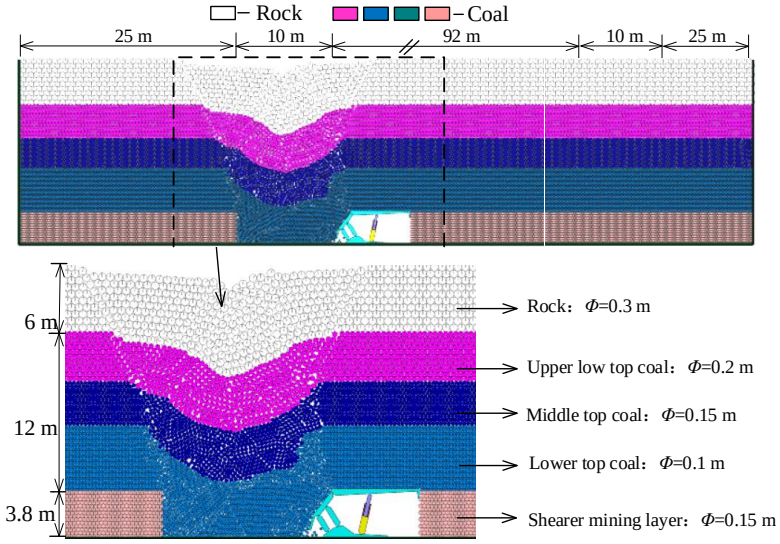

Figure 4 Numerical model

Table 2 Values of the coal particle mechanical parameters adopted in this study

Stratum	Density (kg/m^3)	Elastic modulus (Pa)	Poisson's ratio	Tensile strength (Pa)	Cohesion (Pa)	Internal friction (°)	Local damping coefficient
Coal seam	1373	2.8×10^8	0.3	0	0	44.8	0.05
Gangue layer in coal seams	1800	4.2×10^8	0.25	0	0	35.8	0.05
Immediate roof	2542	18×10^8	0.22	0	0	32.8	0.05

4.2 Numerical simulation scheme

When implementing fully mechanized top-coal drawing technology in the strike direction of a fully mechanized top-coal drawing work face in an extra-thick coal seam, different CSL distances have a significant impact on the top-coal recovery rate, rock content rate, top-coal fragmentation and migration law, and coal-rock interface evolution. To study the influence of different caving step distances on top-coal recovery and the evolution of the coal-rock interface, the numerical simulation uses "rocks appear, close the opening" as the end strip of caving within step distance. During the coal drawing process, the top coal yield of each drawing cycle is statistically analyzed after the initial top-coal caving. In the simulation, the height of the caving coal is 12 m, and the influence of the CSL on the top-coal recovery rate and the evolution characteristics of the coal-rock interface is studied by numerical simulation calculations of fully mechanized top-coal CSLs of 0.6 m, 0.7 m, 0.8 m, 0.9 m, 1.0 m, 1.1 m, 1.2 m, 1.3 m, 1.4 m, 1.5 m, and 1.6 m.

At the same time, the cut hole is opened at 25 m on the left boundary of the numerical model in the direction of the working face. The initial coal drawing is carried out after the advance of 10 m from the open cut. After the initial coal caving, numerical simulation calculations for coal caving step spacings of 0.6 m, 0.7 m, 0.8 m, 0.9 m, 1.0 m, 1.1 m, 1.2 m, 1.3 m, 1.4 m, 1.5 m, and 1.6 m are carried out. The chute area is designated as the termination condition for the current cycle numerical calculation and then continues to excavate forward and move the support model. After the numerical simulation calculation is terminated, the top coal yield within a

single moving frame cycling under different CSLs is counted, the final top-coal recovery rate is calculated, and the top-coal recovery rate is compared with the top-coal recovery rate under different CSLs to determine the optimal caving step distance.

The top-coal and roof are broken into porous bulk with complex structure during the frame moving process of fully mechanized top-coal caving mining. The loose structure caves under the action of gravity. The instantaneous loose effect of coal and rock in the caving process is ignored, and it is simplified as a continuous flowing random loose medium. The boundary line of coal gangue and the equation of the drawing body are deduced by using probability statistics and the calculus method, and the top coal is established. Based on the theoretical calculation model of the recovery rate and rock content, the relationship between the shape evolution law of the top-coal drawing body and the recovery rate of top coal is studied[34][35].

The numerical model uses particle flow to simulate the fully mechanized caving mining process along the direction of the working face. To simplify and facilitate the numerical simulation calculation, basic assumptions are made on the drawing top-coal strata [36][37]:

a. The top coal is loose and broken and does not bear tensile stress;
b. The top coal is regarded as a quasi-rigid body;
c. The hydraulic support only bears the weight of the broken top coal and rock layer above;
d. In the top-coal drawing process, there is no wall spalling or roof falling at the end face.

5 Numerical analysis of a reasonable coal caving step in the direction of the working face

5.1 Evolution analysis of the coal gangue interface

Fig. 5 shows the development of the top-coal drawing body in the initial drawing. In the initial stage of top-coal drawing, the top coal is fully drawn out, and the ellipsoid of top-coal drawing is affected by the tail beam and shield beam of the hydraulic support for top-coal drawing, showing the shape of a cutting variant ellipsoid. For the first coal drawing at the end, the coal drawing funnel is fully developed, and the influence of the top-coal drawing hydraulic support deflects to one side of the goaf.

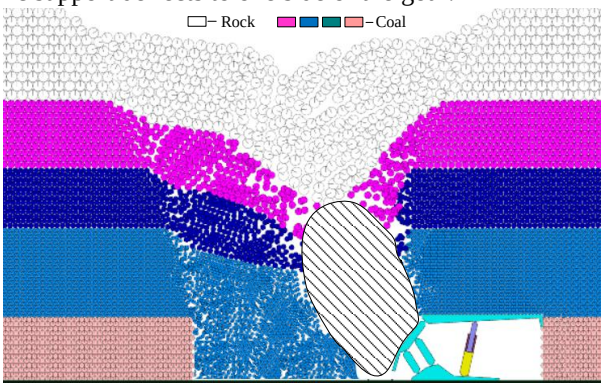

Figure 5 The top-coal caving body shape

Taking 0.8 m and 1.4 m top-coal drawings as an example, in Fig. 6 below, the evolution of the coal-rock boundary under the condition of different drawing CSLs during the top-coal drawing process can be clearly seen. The coal-rock boundary on the side of the goaf is fully developed to the rear of the goaf, and the coal-rock boundary on the side of the coal wall is affected by the hydraulic support and becomes steeper, showing a hook-like shape. Under the condition of 12.0 m top-coal thickness, the coal-rock boundary with 0.8 m and 1.4 m coal drawing CSLs is compared. When the coal drawing CSL is 1.4 m, the back hook of the coal-rock boundary on one side of the coal wall to the goaf side is more obvious. It is revealed that the coal drawing CSL has an effect on the deflection angle of the development of the coal drawing ellipsoid and then affects the evolution of the coal-rock decomposition line; as the work face continues to move forward, the top coal above the hydraulic support will reach the coal drawing opening earlier than the top coal behind the hydraulic support, resulting in strip coal loss.

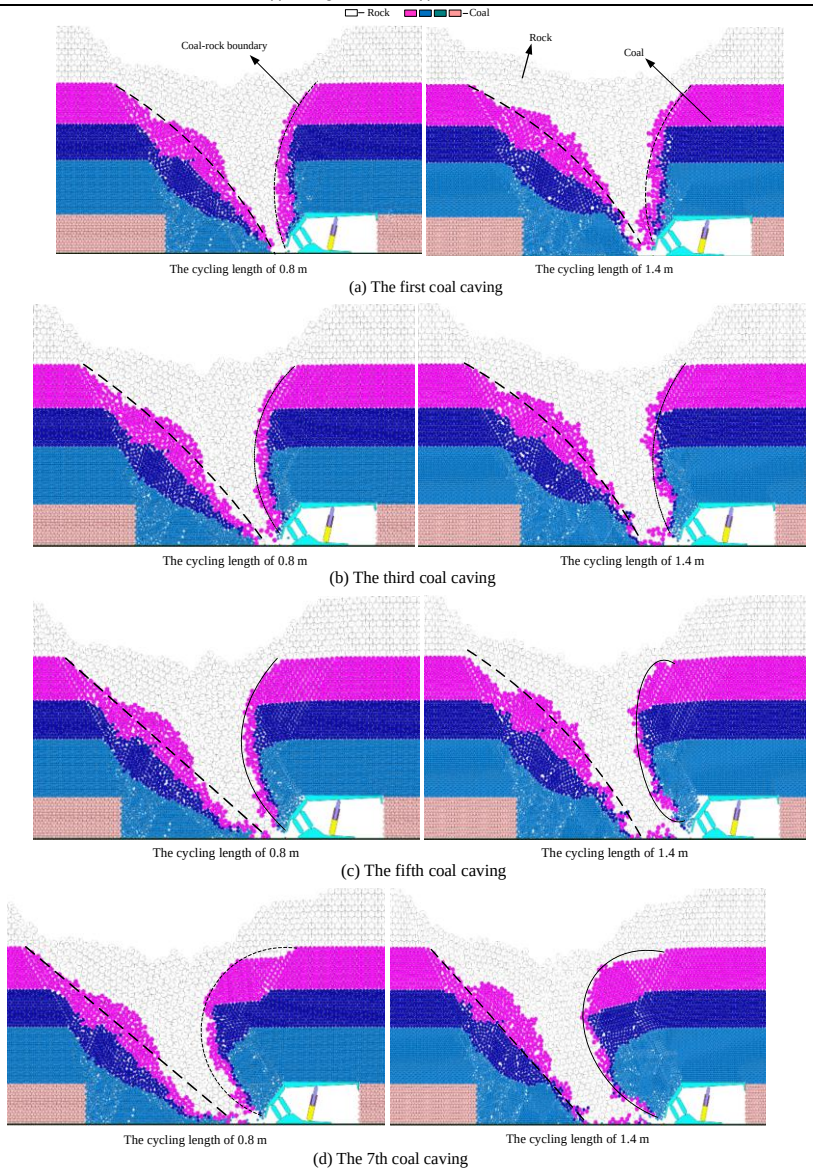

Figure 6 Evolution of the rock-coal interface during the first 7 top-coal drawing cycles

When the coal drawing hydraulic support starts to advance, the funnel shape formed by the interface between the coal drawing ellipsoid and the coal-rock interface is affected by the coal drawing hydraulic support, and only a small amount of top coal above the hydraulic support flows to the coal drawing opening. With the continuous advance of the working face, the top-coal yield at the side of the coal wall increases gradually, and the coal-rock boundary line is extruded by the top-coal drawing body, which fully develops to the goaf side horizontally and changes vertically irregularly. When the working face continues to advance, the top coal on the side of the coal wall begins to be released before the top coal behind the hydraulic support, resulting in the rock above the hydraulic support reaching the coal drawing opening in advance, so a part of the top coal on the side of the goaf will be left in the goaf. With the advance of the working face, the boundary of coal and rock on the side of the coal wall develops laterally to the side of goaf again and becomes tortuous and irregular from the loose extrusion of top coal in the longitudinal direction, which forms a cycle of "upper top coal preferentially discharging – upper rock arriving at the coal drawing opening before the rear top coal – top coal remaining – upper top coal developing towards the goaf", resulting in part of the top-coal circulation remaining in the goaf. In Fig. 7 below, it can be clearly seen that the top-coal drawing process along the strike direction of the working face indicates a strip-shaped release rule for the left goaf.

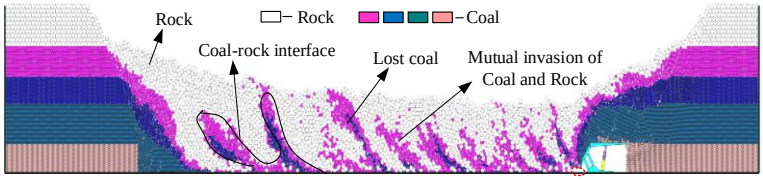

Figure 7 Drawn top-coal caving situation under the cycle step length of 0.8 m

5.2 Determination of the best coal caving step

To analyze the amount of top-coal drawing and the overall top-coal recovery rate in each cycling under different CSL conditions, statistics were made for every cycling under different CSLs under a condition of a 12.0 m top-coal thickness. The discharge amount of top coal in cycling is shown in Fig. 8 below. It can be seen from the broken line graph that under the same top-coal thickness, regardless of the adopted coal drawing CSL, the first top-coal drawing amount is the largest, and within single cycling, the top-coal drawing amount varies with the increase of coal drawing CSL, and the amount of top-coal drawing is relatively increased.

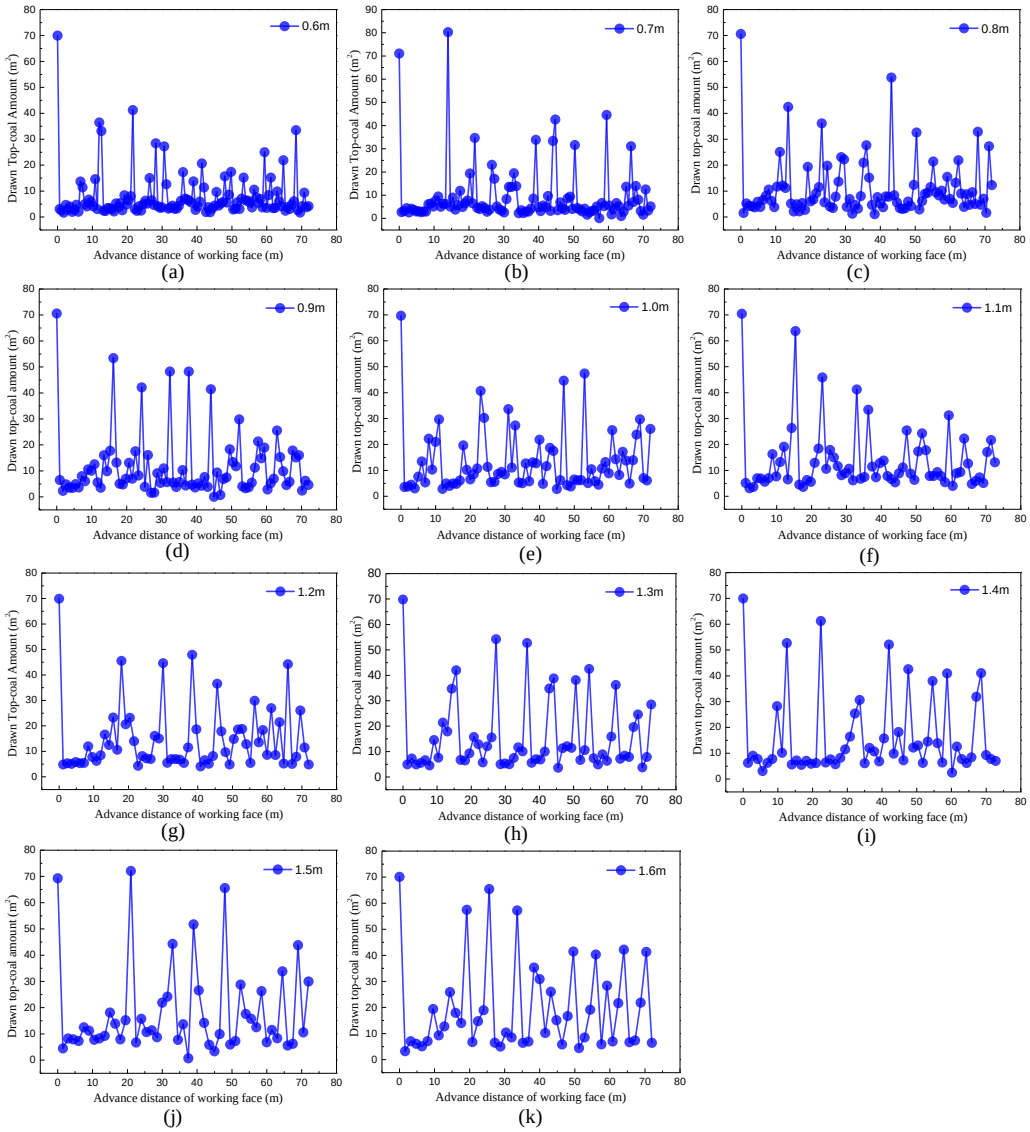

Figure 8 The amount of top-coal drawing at a single CSL under different drawing CSLs

Under the condition of a 12 m top-coal thickness, the dispersion degree of top-coal yield in each moving support length is different. The average value and standard deviation of the top-coal yield in each moving support length are 7.973025, 9.261808, 10.93403, 11.60304, 13.34197, 13.76299, 14.89308, 15.92649, 16.44757, 18.09267, 19.65083, and 9.279914, 32.03684, 11.41444, 12.79514, 12.14694, 12.8423, 13.01509,

14.76194, 15.91162, 17.13303, 17.85377. As shown in Fig. 9 below, it can be clearly seen in the figure that under a top-coal thickness of 12.0 m, the dispersion degree of the top-coal yield in different drawing CSLs is different. Under the condition of a 0.8 m top-coal drawing CSL, the top-coal yield within the single support CSL is the highest average. In Fig. 9(b), it can be seen that with the continuous advance of the working face, the top-coal drawing amount increases steadily. Under the condition of a 0.8 m top-coal drawing CSL, the increase in top-coal drawing is the most linear, and the final yield is the largest. The larger the difference in top-coal yield between the coal drawing openings is, the greater the fluctuation of coal-rock decomposition surface evolution. At the same time, it can be seen that the higher the height of the left triangle coal is, the more coal that is lost. Therefore, under the condition of a 0.8 m coal drawing CSL, the coal-rock interface is the gentlest, and the coal loss is the least.

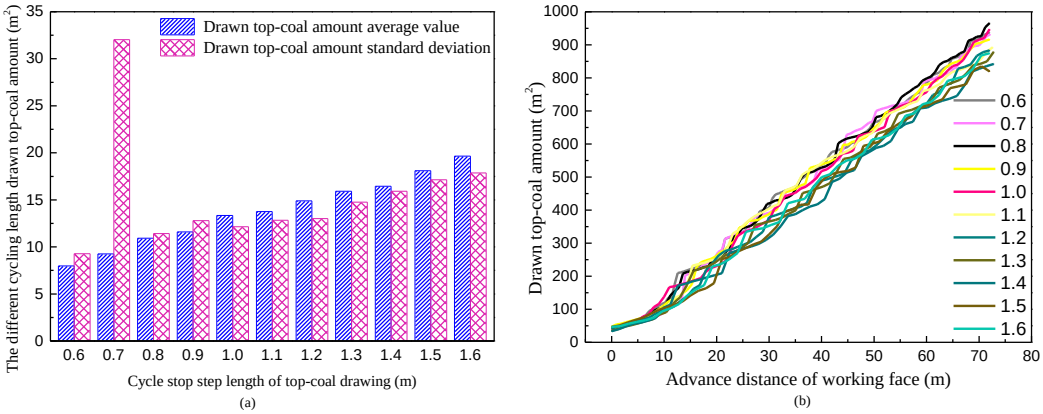

Figure 9 (a) Comparison of the average value and standard deviation of top-coal discharge within a single moving step of different coal drawing CSLs
(b) Variation diagram of top-coal discharge with increasing advancing distance

Using the method of numerical simulation analysis, it can be seen that different results for different coal drawing CSLs can be obtained solely by analyzing the initial position of the working face and advancing to the stop position. Various types of methods are used to advance the mining and adjust the different drawing CSLs, and the total moving distance is basically the same, at approximately 92 m. Under the 12.0 m top-coal thickness and different coal drawing CSL conditions, the particle area of the top-coal drawing area before the start of coal drawing requires a total of approximately 1000 m^2 of top-coal storage capacity. The total area of the model particles is 2185.378 m^2; the total area of the particles at the end of coal drawing, the area difference between the particles at the two ends before the beginning of the coal drawing and the end of the coal drawing, and the area of the top-coal particles is calculated. The top-coal at 12.0 m is the calculated thickness under the conditions of different drawing CSLs, the ratio of the area of the particles discharged from the top-coal drawing area to the area of the top-coal drawing area, and the size of the top-coal recovery rate, as shown in Table 3. The top-coal recovery rates from 11 different drawing CSLs are compared and shown in Fig.10 below.

Table 3 Statistical Table of Top-coal Recovery Rate

Coal drawing CSL/m	Total area of initial state body/m^2	Total surface area of sphere of top-coal drawing area/m^2	Total area of sphere at the end of coal drawing/m^2	Area of more release at both ends/m^2	Area of the sphere released in the coal drawing area/m^2	Top-coal recovery rate/%
0.6	2185.378	995.2016	1220.642	86.1033	878.6327	88.2869
0.7	2185.378	9956414	1222.15	106.555	856.673	86.0423
0.8	2185.378	995.2016	1190.381	107.364	887.633	89.1913
0.9	2185.378	995.2016	1245.532	64.4498	875.3962	87.9617
1.0	2185.378	995.2016	1211.414	100.8845	873.0795	87.7289
1.1	2185.378	1001.689	1263.258	58.8028	863.3172	86.1862
1.2	2185.378	995.2016	1276.9	64.9761	843.5019	84.7569
1.3	2185.378	1003.817	1277.568	75.3826	832.4274	82.9262
1.4	2185.378	1003.817	1313.657	70.6152	801.1058	79.806
1.5	2185.378	995.2016	1298.837	66.7118	819.8292	82.3782

1.6	2185.378	995.2016	1281.44	65.2274	838.7106	84.2754

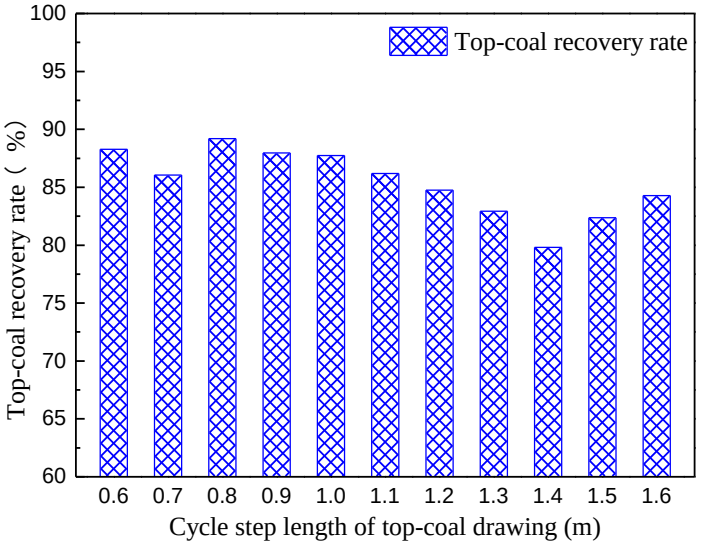

Figure 10 Change in the top-coal recovery rate under different cycle step lengths

Fig.10 shows that the top-coal recovery rate of 12.0 m top coal varies under different caving step conditions. It can be seen in the figure that the top-coal recovery rate is 0.8 m~1.4 m. When the coal drawing CSL is used, the top-coal recovery rate has a steady downward trend. When the coal drawing CSL is 1.4 m to 1.6 m, the top-coal recovery rate rises steadily. Therefore, under the condition of 12.0 m top-coal thickness, the top-coal recovery rate can reach 89.12% when the 0.8 m caving step is adopted. Therefore, it is finally determined that the 0.8 m drawing CSL is the optimal coal drawing CSL for the 15.6 m extra-thick seam of the 8222 fully mechanized caving face in the Tashan Mine.

6 Conclusion

In this study, a particle-block element coupling approach is implemented to investigate a reasonable cycle step length of top-coal drawing for extra-thick coal seams. The block mesh model and the constitutive law of hydraulic support are proposed, and the interaction principle between particles and block elements is introduced. The correlation between the top-coal recovery rate and the shape of the coal-rock interface is analyzed, and based on this result, a reasonable CSL for extra-thick coal seams is determined. The main conclusions are as follows:

(1) By comparing the numerical simulation result to the Bergmark-Roos analytical result, the proposed numerical model is verified and shows good performance in modeling top-coal caving. A 2-D numerical model of hydraulic support considering the mechanical behavior of the legs is established, which can be used for modeling the interactions between hydraulic support and top coals during the top-coal drawing process.

(2) When advancing the process of coal caving support, with the rock reaching the coal drawing opening and with periodic floating, the top-coal drawing body is affected by the tail beam of the hydraulic support, which takes the shape of a cutting variation ellipsoid. In addition, the displacement angle of the ellipsoid to one side of the goaf is different with different CSLs. If the CSL is too long, the upper rock will arrive at the coal drawing opening before the coal behind the hydraulic support. If the coal drawing CSL is too short, the rock in the goaf will rush into the coal drawing opening in advance. As a result, the loss of top coal is periodically inclined to one side of the goaf. In each drawing cycle, the top coal flows regularly twice. The first flow is a large range of top-coal falling after the support movement, and the other flow is the process of top coal upper rock flowing with the top coal at the coal drawing opening.

(3) Combined with the actual geological situation of the no. 8222 working face, the top-coal recovery rate, the shape of the top-coal drawing body, and the evolution characteristics of the coal-rock interface under different CSL conditions are compared. In addition, the mechanism of the lost top coal affected by the CSL is revealed. The results show that the CSL of top-coal drawing has a significant effect on the morphology of the coal-rock interface and the mutual invasion of coal and rock, which is also the primary reason for coal loss and further affects the top-coal recovery rate and the rock-mixing rate. It is suggested that the CSL should be 0.8 m when the top-coal thickness is 12 m when using the form of

"drawing top coal once per reamer".

7 Declaration of competing interest

I declare that I do not have any commercial or associative interest representing a conflict of interest in connection with the paper submitted.

8 Acknowledgement

This study was supported by the National Key R&D Program of China (2018YFC0604502) and China Postdoctoral Science Foundation (2020M672227).

References

[1]. Wang JC, Yang SL, Li Y, et al. Caving mechanisms of loose top coal in longwall topcoal caving mining method. Int J Rock Mech Min Sci. 2014;71:160–170 https://doi.org/10.1016/j.ijrmms.2014.04.024.
[2]. Yang SL, Zhang JW, Chen Y, et al. Effect of upward angle on the drawing mechanismin longwall top coal caving mining. Int J Rock Mech Min Sci. 2016;85:92–101 https://doi.org/10.1016/j.ijrmms.2016.03.004.
[3]. Xie YS, Zhao YS. Numerical simulation of the top coal caving process using thediscrete element method. Int J Rock Mech Min Sci. 2009;46:983–991 https://doi.org/10.1016/j.ijrmms.2009.03.005.
[4]. Yasitli NE, Unver B. 3D numerical modeling of longwall mining with top coal caving.Int J Rock Mech Min Sci. 2005;42:219–235 https://doi.org/10.1016/j.ijrmms.2004.08.007.
[5]. Ediz IG, Dixon-Hardy DW, Akcakoca H, et al. Application of retreating and caving longwall (top coal caving) method for coal production at GLE Turkey. Min Technol.2013;115:41–48 https://doi.org/10.1179/174328606X103586.
[6]. Wang JC. Engineering practice and theoretical progress of top coal caving mining technology in China. J China Coal Soc. 2018;43:43–51 https://doi.org/10.13225/j.cnki.jccs.2017.4101.
[7]. Wang GF, Pang YH, Ma Y, et al. Automated mining technology and equipment forfully-mechanized caving mining with large mining height in extra-thick coal seam. Coal Eng. 2018;50:1–6 https://doi.org/10.11799/ce201801001.
[8]. Ma Y. Study on automatic top coal caving system in fully-mechanized coal caving face. Coal Sci Technol. 2013;41: 22–24 https://doi.org/10.13199/j.cnki.cst.2013.11.019.
[9]. Wang GF, Pang YH, Ren HW, et al. Coal safe and efficient mining theory, technology and equipment innovation practice. J China Coal Soc. 2018;43:903–913 https://doi.org/10.13225/j.cnki.jccs.2017.1705.
[10]. Wang GF, Wang H, Ren HW, et al. 2025 scenarios and development path of intelligent coal mine. J China Coal Soc. 2018;43: 5–305 https://doi.org/10.13225/j.cnki.jccs.2018.0152.
[11]. Vakili A, Hebble white BK. A new cavability assessment criterion for Longwall Top Coal Caving. Int J Rock Mech Min Sci. 2010;47: 1317–1329 https://doi.org/10.1016/j.ijrmms.2010.08.010.
[12]. Wu J, Zhang Y. Study on the basic theory of longwall top coal caving system. J China Univ Min Technol. 1998; 27:331–335 http://www.cnki.com.cn/Article/CJFDTotal-ZGKD804.000.htm.
[13]. Yan SH, Wu J. Analysis of top coal movement and damage characteristics in top coal caving. J China Coal Soc. 1996;15: 155–162 http://www.cnki.com.cn/Article/CJFDTotal-YSLX602.010.htm.
[14]. Wu J. Theory and practice of sub-level caving method in China. J China Coal Soc.1991;3:1–11 https://doi.org/10.13225/j.cnki.jccs.1991.03.001.
[15]. Wang JC, FU Q. The loose medium flow field theory and its application on the longwall top coal caving. J China Coal Soc. 2002;27:337–341 https://doi.org/10.3321/j.issn:0253-9993.2002.04.001.
[16]. Wang JC, Li ZG, Chen YJ, et al. The experimental study of loose medium flow field on the longwall top coal caving. J China Coal Soc. 2004;29:260–263 https://doi.org/10.13225/j.cnki.jccs.2004.03.002.
[17]. Wang JC, Zhang JW, li ZL. A new research system for caving mechanism analysis andits application to sublevel top coal caving mining. Int J Rock Mech Min Sci.2016;88:273–285 https://doi.org/10.1016/j.ijrmms.2016.07.032.
[18]. Wang JC, Song ZY, Zhang JW, et al. Three-dimensional experimental study of loose top coal drawing law for longwall top coal caving mining technology. J Rock Mech and Geo Eng. 2015;7:318–326 https://doi.org/10.1016/j.jrmge.2015.03.010.
[19]. Khanal M, Adhikary D, Balusu R. Evaluation of mine scale longwall top coal caving parameters using continuum analysis[J]. Mining Science and Technology (China), 2011, 21(6): 787-796. https://doi.org/10.1016/j.mstc.2011.06.027
[20]. Khanal M, Adhikary D, Balusu R. Prefeasibility study-geotechnical studies for introducing longwall top coal caving in Indian mines[J]. Journal of Mining Science, 2014, 50(4): 719-732.https://doi.org/10.1134/S1062739114040139

[21]. Unver B, Yasitli N E. Modelling of strata movement with a special reference to caving mechanism in thick seam coal mining [J]. International Journal of Coal Geology, 2006, 66(4): 227-252. https://doi.org/10.1016/j.coal.2005.05.008
[22]. Wang JC, Wei LK, Zhang JW, et al. 3-D numerical simulation on the top coal movement law under caving mining technique. J China Coal Soc.2013; 38:1905–1911 https://doi.org/10.13225/j.cnki.jccs.2013.11.013.
[23]. Vakili A, Hebble white BK. A new cavability assessment criterion for Longwall Top Coal Caving. Int J Rock Mech Min Sci. 2010; 47:1317–1329 https://doi.org/10.1016/j.ijrmms.2010.08.010.
[24]. Liu Chuang, Li Huamin, Zhou Ying, Li Dongyin. Cooperative caving method with multiple caving openings in fully mechanized caving face[J].Journal of China Coal Society,2019,44(09):2632-2640. 10.13225/j.cnki.jccs.2018.1278
[25]. Qunlei Zhang, Jinchao Yue, Chuang Liu, Chun Feng, Huamin Li, Study of automated top-coal caving in extra-thick coal seams using the continuum-discontinuum element method, International Journal of Rock Mechanics and Mining Sciences, Volume 122, 2019, ISSN 1365-1609. https://doi.org/10.1016/j.ijrmms.2019.04.019.
[26]. Feng C, Li SH, Liu XY. A procedure for transiting FEM into DEM and its application. Rock Soil Mech. 2015; 36(4):1027–1034 https://doi.org/10.16285/j.rsm.2015.04.017.
[27]. Potyondy DO, Cundall PA. A bonded-particle model for rock. Int J Rock Mech Min Sci.2004;41:1329–1364. https://doi.org/10.1016/j.ijrmms.2004.09.011.
[28]. ZHANG Q L, ZHI Z H, FENG C, et al. Investigation of concrete pavement cracking under multi-head impact loading via the continuum-discontinuum element method [J]. International Journal of Impact Engineering, 2020.https://doi.org/10.1016/j.ijimpeng.2019.103410
[29]. ZHANG Q, YUAN R, WANG S, et al. Optimizing Simulation and Analysis of Automated Top-Coal Drawing Technique in Extra-Thick Coal Seams [J]. Energies, 2020.https://doi.org/10.3390/en13010232
[30]. Liu Chuang, Li Huamin, Zhang Qunlei. Research on reasonable ratio of setting force to rated working resistance of large mining height hydraulic support[J]. Journal of Mining & Safety Engineering, 2018, 035(004):725-733. https://doi:10.13545/j.cnki.jmse.2018.04.009.
[31]. Wang JC, Song ZY, Zhang JW, et al. Theoretical model of drawing body in LTCC mining. J China Coal Soc. 2016; 41:352–358 https://doi.org/10.13225/j.cnki.jccs.2015.1750.
[32]. Kuchta ME. A revised form of the Bergmark–Roos equation for describing the gravity flow of broken rock. Miner Resour Eng. 2002; 11:349–360 https://doi.org/10.1142/S0950609802001002.
[33]. Melo F, Vivanco F, Fuentes C, et al. On drawing body shapes: from Bergmark–Roos tokinematic models. Int J Rock Mech Min Sci. 2007; 44:77–86 https://doi.org/10.1016/j.ijrmms.2006.04.010.
[34]. Zhang Jinwang, Wang Jiachen, Wei Weijie, Li Lianghui. Experimental study on the effect of fragmentation gradation on the flow characteristics of loose top coal [J]. Journal of China Coal Society, 2019, 44(04): 985-994.https://doi.org/10.3390/en11092274
[35]. Ji Hongguang, Cai Zhenyu, Zhang Biao, Yang Bensheng. Test of caving technology and top coal movement characteristics of fully mechanized caving face in large inclined thick seam [J]. Journal of Mining and Safety Engineering, 2016, 33(02): 208-213. https://doi:10.13545/j.cnki.jmse.2016.02.003.
[36]. Wu Jian, Chen Xuehua. Discrete element simulation study of loose top coal falling law in fully mechanized caving mining [J]. Journal of Liaoning Technical University (Natural Science Edition), 1999, 18(6): 570-573.
https://kns.cnki.net/kcms/detail/detail.aspx?FileName=FXKY199906003&DbName=CJFQ1999
[37]. Huang Bingxiang, Liu Changyou, Wu Fengfeng, et al. Study on the granular model test of coal caving technology under the roof of extremely loose fine sandstone[J]. Journal of China University of Mining and Technology, 2006, 35(3): 351-355.
https://kns.cnki.net/kcms/detail/detail.aspx?FileName=ZGKD200603012&DbName=CJFQ2006